Applied Catalysis A: General 478 (2014) 15–20

Contents lists available at ScienceDirect

Applied Catalysis A: General

journal homepage: www.elsevier.com/locate/apcata

Hydrogen generation from hydrolysis of ammonia borane in the presence of highly efficient poly(*N*-vinyl-2-pyrrolidone)-protected platinum-ruthenium nanoparticles

Murat Rakap*

Department of Chemistry, Yuzuncu Yil University, 65080, Van, Turkey

ARTICLE INFO

Article history:
Received 8 January 2014
Received in revised form 26 February 2014
Accepted 17 March 2014
Available online 25 March 2014

Keywords:
Platinum
Ruthenium
Nanoparticles
Ammonia borane
Hydrogen

ABSTRACT

Herein, the employment of PVP-protected Pt–Ru bimetallic nanoparticles (3.2 ± 1.4 nm) as highly efficient catalysts in the hydrolysis of ammonia borane for hydrogen generation is reported. They were prepared by co-reduction of two metal ions in ethanol/water mixture by an alcohol reduction method and characterized by TEM–EDX analysis, UV–vis spectroscopy, and X-ray photoelectron spectroscopy. They are recyclable and highly active for hydrogen generation from the hydrolysis of ammonia borane even at very low concentrations and temperature, providing a record numbers of average TOF value (308 mol H_2 mol_{cat}^{-1} min^{-1}) and maximum hydrogen generation rate (9884 L H_2 min^{-1} $(mol_{cat})^{-1}$) for ammonia borane. PVP-protected Pt–Ru bimetallic nanoparticles provide activation energy of 56.3 ± 2 kJ mol^{-1} for the hydrolysis of ammonia borane.

1. Introduction

Hydrogen has been considered as a clean and environmentally benign new energy carrier for heating, transportation, mechanical power and electricity generation [1,2], since there is an increasing demand for the renewable energy sources due to the depletion of fossil fuel resources, environmental pollution, and global warming caused by a steep increase in concentration of carbon dioxide and other greenhouse gases in the atmosphere [3–6]. However, the storage of hydrogen is still a challenge for the implementation of hydrogen economy [7]. Among the chemical hydrides tested as solid hydrogen storage materials, ammonia borane (H_3NBH_3, AB) appears to be suitable hydrogen source due to a number of advantageous properties such as the high hydrogen storage capacity (19.6% wt) which meets the US-DOE criteria for hydrogen storage materials [3,8], the optimal control on hydrogen generation rate by supported catalysts, the acceptable hydrogen generation rate even at low temperature, high solubility in water, the availability and easy handling [9,10]. Additionally, it has an advantage of the stability of aqueous solutions to self-hydrolysis, and there is no need to add any base to stabilize the aqueous solutions of AB. AB can liberate hydrogen upon hydrolysis at room temperature in the presence of suitable catalysts according to Eq. (1) [11].

$$H_3NBH_3(aq) + 2H_2O(L) \xrightarrow{\text{catalyst}} NH_4^+(aq) + BO_2^-(aq) + 3H_2(g) \quad (1)$$

Various catalysts including $Ni_{1-x}Pt_x$ hollow spheres [12], Cu@Cu_2O core shell catalysts [13], hollow Ni–SiO_2 nanosphere [14], Fe(0) NPs [15], PVP-protected Ni(0) [16] and Co(0) NCs [17], polymer-stabilized Ru(0) and Pd(0) NCs [18], magnetically recyclable Fe–Ni alloy [19], Co(0) NPs [20], water/air-stable Ni NPs [21], Co–Mo–B/Ni foam [22], hollow Co–B nanospindles [23], nanoparticle-assembled Co–B thin film [24], bimetallic Au–Ni NPs embedded in SiO_2 nanospheres [25], Cu/Co_3O_4 NPs [26], electroless Co–Ni–P/Pd–TiO_2 [27], Pd–PVB–TiO_2 [28], SiO_2 supported monodisperse Ni NPs [29], Co–SiO_2 nanosphere [30], graphene oxide supported Pd NPs [31], and Ru NPs [32] have been tested for the hydrolysis of AB.

Among these catalysts, nanoparticle-types provided good catalytic activities as expected, due to the small particle sizes. However, the addition of second element to the monometallic nanoparticles will definitely improve the catalytic properties [33,34]. Therefore, it has been focused on the employment of highly effective bimetallic-type nanoparticles as catalyst for hydrogen generation from the hydrolysis of AB, recently. To the knowledge, there is no reported work on the catalytic activity of poly(*N*-vinyl-2-pyrrolidone)-protected platinum–ruthenium nanoparticles in the hydrogen generation from the hydrolysis of AB. Herein, the

* Tel.: +90 432 225 10 25.
E-mail addresses: mrtrakap@gmail.com, muratrakap@gmail.com

http://dx.doi.org/10.1016/j.apcata.2014.03.022
0926-860X/

employment of highly efficient PVP-protected Pt–Ru bimetallic nanoparticles (will be referred as Pt–Ru@PVP nanoparticles hereafter) for hydrogen generation from the hydrolysis of AB is reported. They were prepared by an alcohol reduction method [35] and characterized by TEM–EDX analysis, UV–vis spectroscopy, and X-ray photoelectron spectroscopy. Additionally, the formation of PVP-protected Pt–Ru nanoparticles was confirmed by comparing the catalytic activities of monometallic platinum and ruthenium nanoparticles and the physical mixture of them with the catalytic activity of bimetallic nanoparticles.The kinetic studies were carried out depending on the catalyst/substrate concentrations and temperature. Although the cost of noble metal catalysts is assumed to be high, the high catalytic activity and effectivity of the PVP-protected Pt–Ru nanoparticles make them a very promising candidate to be used as catalyst in developing efficient portable hydrogen generation systems using AB as solid hydrogen storage material since it would compensate the cost concerns.

2. Experimental

2.1. Materials

Ruthenium(III) chloride trihydrate ($RuCl_3{\cdot}3H_2O$), hexachloroplatinic(IV) acid hexahydrate ($H_2PtCl_6{\cdot}6H_2O$), poly(*N*-vinyl-2-pyrrolidone) (PVP-40), and ammonia borane (H_3NBH_3) were purchased from Aldrich. Ethanol was purchased from Merck. Deionized water was distilled by a water purification system (Milli-Q system). All glassware and Teflon-coated magnetic stir bars were cleaned with acetone, followed by copius rinsing with distilled water before drying in an oven at 150 °C.

2.2. The preparation of PVP-protected Pt–Ru@PVP nanoparticles

Pt–Ru@PVP nanoparticles were prepared by an alcohol reduction method. First, solutions of ruthenium(III) chloride trihydrate (0.25 mmol in 25 mL ethanol) and hexachloroplatinic(IV) acid hexahydrate (0.25 mmol in 25 mL water) were mixed and poly(*N*-vinyl-2-pyrrolidone) (PVP-40, 2.5 mmol of monomeric units) was added to this solution as a protecting polymer. Then, the mixed solution was refluxed at 90 °C for 2 h. The formed Pt–Ru nanoparticles have brownish black color and stable for months at room temperature. The total concentration of both metals was kept as 5.0 mM in 50 mL of the mixed solution.

2.3. The characterization of Pt–Ru@PVP nanoparticles

2.3.1. UV–vis analysis

UV–vis spectra were recorded on a Cary 5000 (Varian) UV–vis spectrophotometer. A quartz cell with a part length of 1 cm was used and spectra were collected over the range of 200–900 nm.

2.3.2. TEM–EDX analysis

Transmission electron microscopy (TEM) analysis was carried out using a JEOL-2010 microscope operating at 200 kV, fitted with a LaB_6 filament and has lattice and theoretical point resolutions of 0.14 nm and 0.23 nm, respectively. Samples were examined at magnification between 100 and 400 K. One drop of dilute suspension of sample was deposited on the TEM grids and the solvent was then evaporated. The diameter of each particle was determined from the enlarged photographs.

2.3.3. X-Ray photoelectron spectroscopy

X-ray photoelectron spectrum (XPS) of the isolated nanoparticles was taken by using SPECS spectrometer equipped with a hemispherical analyzer and using monochromatic Mg-*K*α radiation (1250 eV, the X-ray tube working at 15 kV and 350 W).

2.3.4. ^{11}B NMR spectra

^{11}B NMR spectra were recorded on a Bruker Avance DPX 400 with an operating frequency of 128.15 MHz for ^{11}B. D_2O and $BF_3{\cdot}(C_2H_5)_2O$ were used as a lock and external reference, respectively. At the end of the hydrolysis reaction, the resulting solutions were filtered and the filtrates used for taking ^{11}B NMR spectra.

2.4. Method to test the catalytic activity of Pt–Ru@PVP nanoparticles in the hydrolysis of AB

The catalytic activity of Pt–Ru@PVP nanoparticles in the hydrolysis of AB in aqueous solution was determined by measuring the rate of hydrogen generation. In all the experiments, a jacketed reaction flask (50 mL) containing a Teflon-coated stir bar was placed on a magnetic stirrer (Heidolph MR-301) and thermostated to 25.0 ± 0.1 °C by circulating water through its jacket from a constant temperature bath. Then, a graduated glass tube (40 cm in height and 2.5 cm in diameter) filled with water was connected to the reaction flask to measure the volume of the hydrogen gas to be evolved from the reaction. In a typical experiment, 63.6 mg (2 mmol) of H_3NBH_3 was dissolved in 20 mL of water. The solutions were transferred with a glass pipet into the reaction flask thermostated at 25.0 ± 0.1 °C. Then, aliquots of Pt–Ru@PVP nanoparticles from the stock solution (5.0 mM) were added into the reaction flask. The experiment was started by closing the flask and the volume of hydrogen gas evolved was measured by recording the displacement of water level at the stirring speed of 900 rpm. In addition to the volumetric measurement of the hydrogen evolution, the conversion of AB ($\delta = -23.9$ ppm) [11] to metaborate ($\delta = 9$ ppm) [36] was also checked by ^{11}B NMR spectroscopy.

2.5. Determination of activation energy of Pt–Ru@PVP nanoparticles in the hydrolysis of AB

In a typical experiment, the hydrolysis of AB (100 mM) catalyzed by Pt–Ru@PVP nanoparticles (0.3 mM) was performed by following the same procedure described in Section 2.4 at various temperatures (10, 15, 20, 25, and 30 °C) to obtain the activation energy (E_a).

2.6. Recyclability of Pt–Ru@PVP nanoparticles in the hydrolysis of AB

The recyclability of Pt–Ru@PVP nanoparticles in the hydrolysis of AB was determined by a series of experiments started with a 20 mL solution containing 0.3 mM Pt–Ru@PVP nanoparticles and 0.100 M AB at 25.0 ± 0.1 °C. When the complete conversion is achieved, another equivalent of AB was immediately added to the reaction mixture. The results were expressed as % initial catalytic activity of Pt–Ru@PVP nanoparticles versus the number of catalytic runs in the hydrolysis of AB solution.

3. Results and discussion

3.1. Preparation and characterization of PVP-protected Pt–Ru nanoparticles

Pt–Ru@PVP nanoparticles were prepared from the co-reduction of mixture of hexachloroplatinic(IV) acid hexahydrate and ruthenium(III) chloride trihydrate by an alcohol reduction method in the presence of PVP in ethanol–water mixture at refluxing temperature. PVP serves as stabilizer and reducing agent. After refluxing

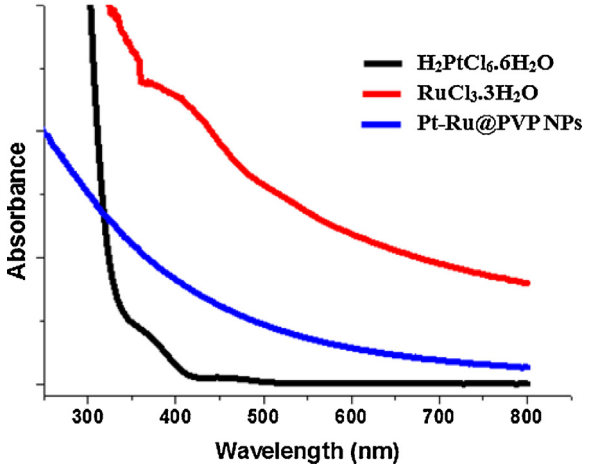

Fig. 1. UV–vis absorption spectra of the aqueous solutions of $H_2PtCl_6{\cdot}6H_2O$, $RuCl_3{\cdot}3H_2O$, and Pt–Ru@PVP nanoparticles.

for 2 h, the color of the solution turned to brownish black, indicating the reductions of Pt^{4+} and Ru^{3+} ions to Pt^0 and Ru^0 to form nanoparticles of them. Monitoring the UV–vis electronic absorption spectra of the solution provides the best way to follow this conversion. Fig. 1 shows the spectral change during the formation of Pt–Ru@PVP nanoparticles from the reduction corresponding platinum and ruthenium salts by PVP. The absorption bands due to d–d transitions in Pt^{4+} and Ru^{3+} ions completely disappear after refluxing the solution, indicating the complete reduction of the corresponding ions. The catalyst was found to be highly stable for weeks with any precipitation of the metal particles at room temperature.

The size, morphology and composition of Pt–Ru@PVP nanoparticles were investigated by TEM–EDX analyses. Fig. 2 shows the TEM images taken at different magnifications (a—50, b—20, c—2 nm, and d—after fifth hydrolysis run) and the EDX spectrum (Fig. 2e) of Pt–Ru@PVP nanoparticles, confirming alloy structure and 1:1 ratio of Pt:Ru. 1:1 ratio of Pt:Ru was also confirmed by ICP analysis. The mean particle size was determined as 3.2 ± 1.4 nm from TEM images by counting 226 non-touching particles.

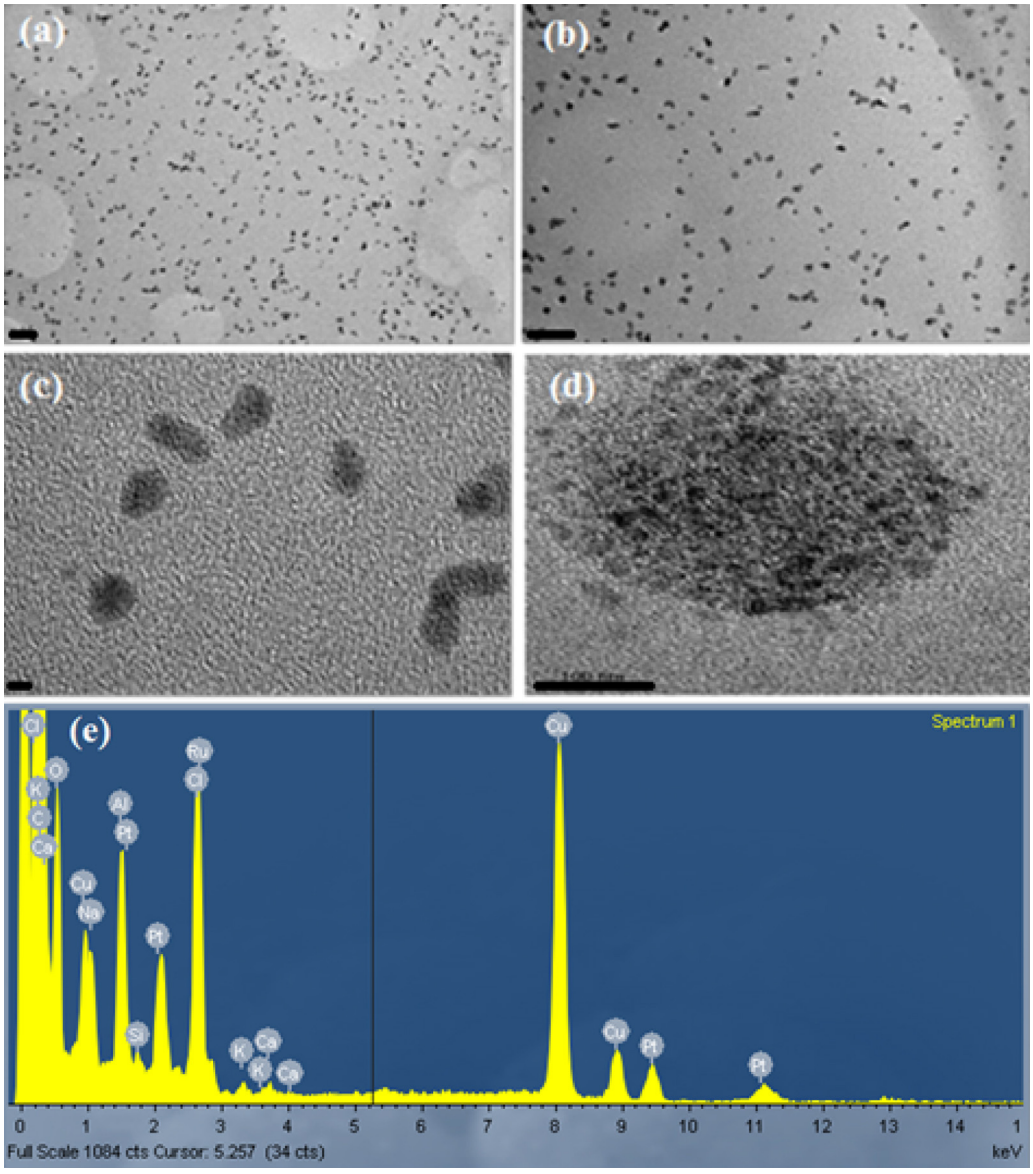

Fig. 2. TEM images ((a) 50, (b) 20 nm, (c) 2 nm, and (d) after fifth hydrolysis run) and the EDX spectrum (e) of Pt–Ru@PVP nanoparticles.

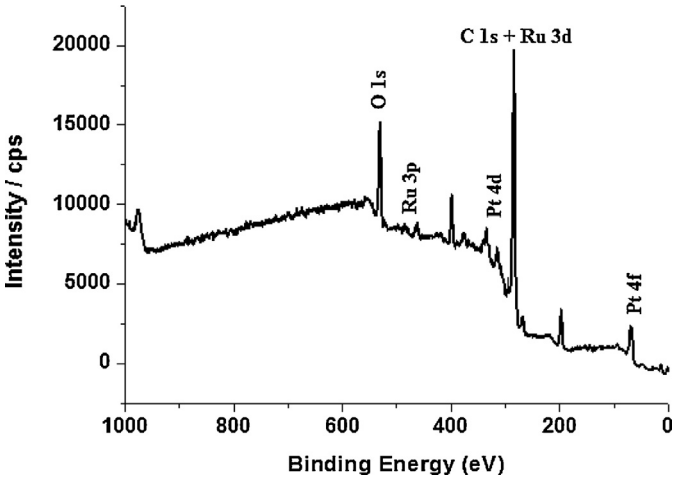

Fig. 3. X-Ray photoelectron spectrum of Pt–Ru@PVP nanoparticles.

The PVP-protected Pt–Ru@PVP nanoparticles were isolated by evaporating all the solvent. The isolated samples of the catalyst were used for the XPS analysis of the catalyst surface. The main peaks observed in the survey scan XPS (Fig. 3) are C 1s, Pt 4d, Pt 4f, Ru 3d, Ru 3p, and O 1s located at 285, 320–350, 65–80, 280–285, 460–480, and 530 eV, respectively. The XPS spectra for Pt 4f are characterized by a doublet containing a binding energy of 70.3 eV for $4f_{7/2}$ and 73.8 eV for $4f_{5/2}$, confirming the presence Pt(0) [37]. Due to the overlap of the C 1s and Ru 3d peaks around 285 eV, it is very difficult to analyze this region for ruthenium properly. The peak located at 462 eV for Ru $3p_{3/2}$ is readily assigned to the Ru(0) [38]. There is no higher oxidation state peaks for both metals of the catalyst in the XPS spectra, indicating the protection of Pt(0) and Ru(0) species by the attachment of PVP during catalyst preparation procedure.

Additionally, the formation of PVP-protected Pt–Ru nanoparticles rather than the physical mixtures of individual monometallic nanoparticles was confirmed by comparing the catalytic activities of all the types (monometallic Pt and Ru nanoparticles, 1:1 physical mixture of them, and 1:1 Pt–Ru bimetallic nanoparticles) in the hydrolysis of AB. As shown in Fig. 4, Pt–Ru@PVP nanoparticles provided a much higher catalytic activity than the physical mixture of Pt and Ru monometallic nanoparticles, clearly indicating that the prepared catalyst is composed of Pt–Ru@PVP bimetallic

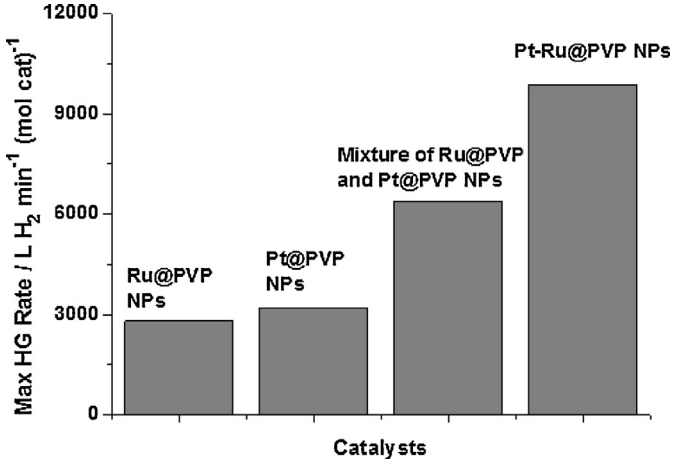

Fig. 4. Comparison of the catalytic activities of 0.3 mM of Pt and Ru monometallic nanoparticles, physical mixture of them, and Pt–Ru@PVP bimetallic nanoparticles in the hydrolysis of 0.100 M AB at 25.0 ± 0.1 °C.

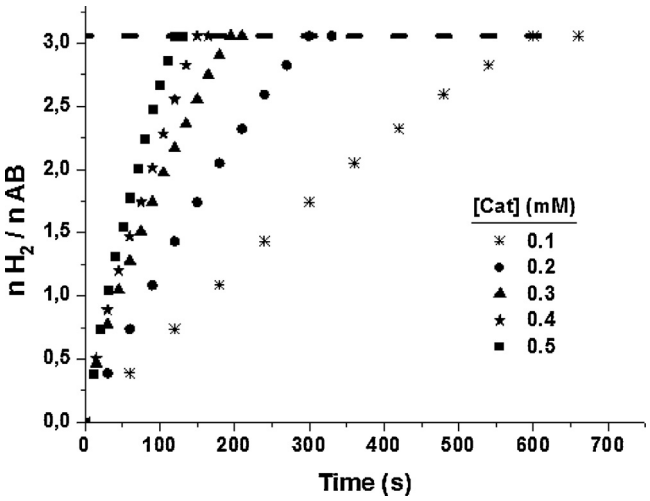

Fig. 5. Plot of mol H_2 mol^{-1} AB versus time for the hydrolysis of 0.100 M AB solutions in the presence of Pt–Ru@PVP nanoparticles in different catalyst concentrations (0.1, 0.2, 0.3, 0.4, and 0.5 mM) at 25.0 ± 0.1 °C.

nanoparticles rather than a mixture of the individual monometallic nanoparticles. This much higher catalytic activity of bimetallic nanoparticles stems from the synergistic effects of platinum and ruthenium [33] and the reduced particles size compared to the individual platinum (4.6 nm) and ruthenium (4.2 nm) nanoparticles.

3.2. Testing the catalytic activity of Pt–Ru@PVP nanoparticles in the hydrolysis of AB

Pt–Ru@PVP nanoparticles were found to be highly efficient catalyst for the hydrolysis of AB. Fig. 5 shows the plots of the volume of generated hydrogen gas versus time (plot of mol H_2 mol^{-1} AB versus time) in the catalytic hydrolysis of 0.100 M AB solutions in the presence of Pt–Ru@PVP nanoparticles in different catalyst concentrations at 25.0 ± 0.1 °C. The linear hydrogen generation starts immediately without an induction period and continues until the complete hydrolysis of AB. The quantity of ammonia liberated during the hydrolysis of AB has been found to be negligible when the catalyst and substrate concentrations are lower than 0.06 mol% and 6 wt%, respectively [39]. As expected, the control tests using copper(II) sulfate trap with acid–base indicators resulted in no NH_3 evolution in detectable amount in the experiments conducted in this study. Additionally, conversion of AB (δ = −23.9 ppm) to metaborate (δ = 9 ppm) was also checked by ^{11}B NMR spectroscopy (Fig. 6). The signal of external reference, $BF_3{\cdot}(C_2H_5)_2O$, at 0 ppm is not shown in the figure.

Fig. 7 shows the plots of the volume of generated hydrogen gas versus time in the catalytic hydrolysis of 0.100 M AB solutions in the presence of Pt–Ru@PVP nanoparticles (0.3 mM) at various temperatures (in the range of 10–30 °C). It is worth to note that using Pt–Ru@PVP nanoparticles (0.3 mM) leads to complete hydrogen release (3.0 mol H_2 mol^{-1} AB) for the hydrolysis of AB within 195 s, corresponding to record average TOF value of 308 mol H_2 mol_{cat}^{-1} min^{-1} and maximum hydrogen generation rate of 9884 L H_2 min^{-1} $(mol_{cat})^{-1}$ at 25.0 ± 0.1 °C. The TOF values of various catalysts in the hydrolysis of AB are given in Table 1, for comparison.

The rate constants of hydrogen generation from the hydrolysis of AB were calculated from the linear portions of the plots given in Fig. 7 at five different temperatures and used for the calculation of the activation energy (E_a = 56.3 ± 2 kJ mol^{-1} for the hydrolysis of AB) from the Arrhenius plot (Fig. 8) for hydrolysis reaction. This activation energy of 56.3 ± 2 kJ mol^{-1} for the hydrolysis of AB is

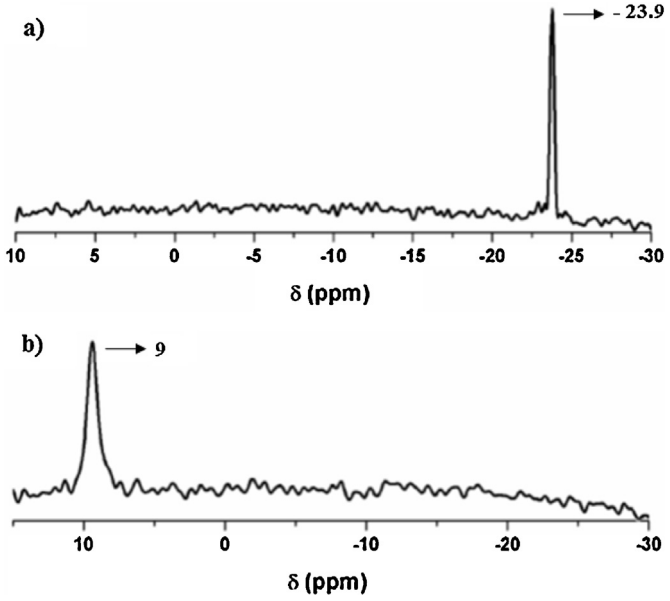

Fig. 6. ^{11}B NMR spectrum (a) before and (b) after hydrolysis of 0.100 M AB catalyzed by 0.3 mM Pt–Ru@PVP nanoparticles.

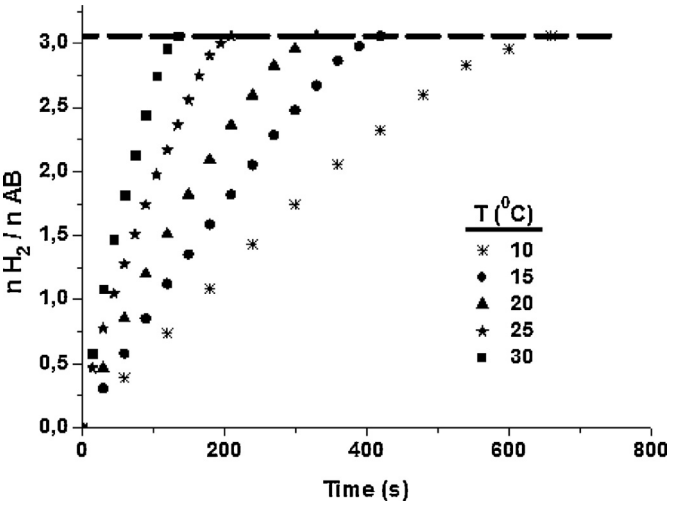

Fig. 7. Plots of the volume of generated hydrogen gas versus time in the catalytic hydrolysis of 0.100 M AB solutions in the presence of Pt–Ru@PVP nanoparticles (0.3 mM) at various temperatures (10, 15, 20, 25, and 30 °C).

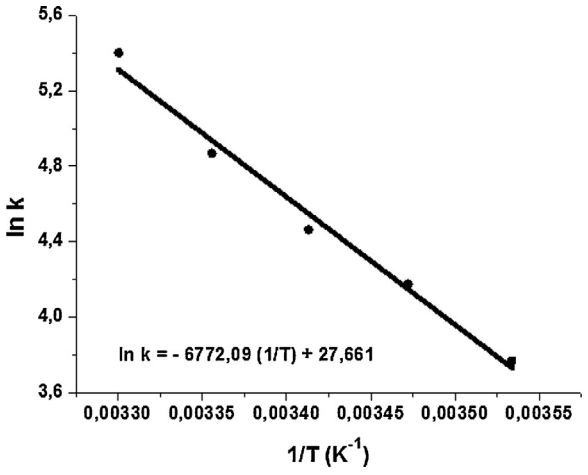

Fig. 8. Arrhenius plot for the hydrolysis of AB (0.100 M) catalyzed by 0.3 mM Pt–Ru@PVP nanoparticles.

Table 1
Activities in terms of TOF values of various catalyst systems tested in hydrogen generation from the hydrolysis of AB (The TOF values were either directly taken or estimated from the data given in respective references.).

Catalyst	TOF (mol H_2 mol catalyst^{-1} min^{-1})	Reference
Pt–Ru@PVP NPs	308.0	This study
Laurate-stabilized Rh(0) NCs	200.0	[46]
Zeolite-Rh(0) NCs	92.0	[47]
Laurate-stabilized Ru(0) NCs	75.0	[48]
Pt/C	55.4	[49]
Co	44.2	[20]
In-situ Co(0) NPs	39.8	[16]
Ru@Al_2O_3 NPs	39.6	[32]
$Co_{35}Pd_{65}$/C	35.7	[50]
RGO-Pd NPs	26.3	[31]
PSSA-*co*-MA stabilized Co(0) NCs	25.7	[44]
PtO_2	20.8	[49]
Graphene-Pd(0) NPs	15.5	[51]
Pt black	13.9	[49]
Au@Co core–shell NPs	13.7	[52]
In-situ $Fe_{1-x}Ni_x$ NPs	10.9	[21]
PSSA-*co*-MA stabilized Ni(0) NCs	10.1	[44]
Electroplated Co–P	10.0	[36]

lower than the activation energies reported in the literature for the same reaction using many different catalysts: 70 kJ mol^{-1} for bulk nickel [40], 63 kJ mol^{-1} for PVP-stabilized cobalt(0) nanoclusters [17], but still higher than 56 kJ mol^{-1} for zeolite confined palladium(0) nanoclusters [41], 52 kJ mol^{-1} for Ni–Ag/C [42], 39 kJ mol^{-1} for $Pt_{0.65}Ni_{0.35}$ nanoparticles [43], 44 kJ mol^{-1} for PSSA-*co*-MA stabilized Pd(0) nanoclusters [44], 44 kJ mol^{-1} for (Co–Mo–B)/Ni foam [22], and 34 kJ mol^{-1} for SiO_2-supported monodisperse nickel nanoparticles [29].

3.3. Recyclability of Pt–Ru@PVP nanoparticles in the hydrolysis of AB

The recyclability of Pt–Ru@PVP nanoparticles in the hydrolysis of AB was investigated by successive additions of AB after the first cycle of the hydrolysis reaction. Fig. 9 shows the results of the recyclability tests for the hydrolysis of AB catalyzed by Pt–Ru@PVP nanoparticles. The Pt–Ru@PVP nanoparticles catalyst retains 72% of its initial catalytic activity in the hydrolysis of AB, even at the fifth run. The decrease in the catalytic activity of Pt–Ru@PVP nanoparticles in the hydrolysis of AB is due to the passivation of nanoparticles' surface by increasing amount of metaborate, which

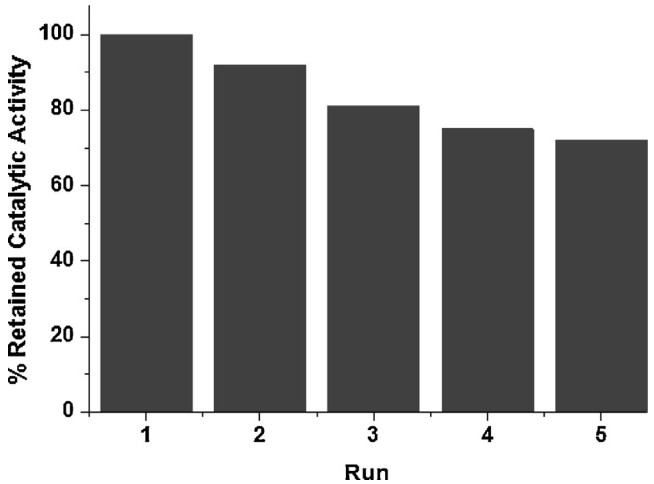

Fig. 9. Retained % catalytic activity of 0.3 mM Pt–Ru@PVP nanoparticles in the successive catalytic runs for the hydrolysis of 0.100 M AB at 25.0 ± 0.1 °C.

decreases accessibility of active sites [45] and the aggregation of nanoparticles as shown in the TEM image of the catalyst taken after fifth run of the hydrolysis reaction (Fig. 2d).

4. Conclusions

In summary, our study of the preparation, characterization, and employment of Pt–Ru@PVP nanoparticles as catalyst for the hydrolysis of AB has led to the following conclusions and insights:

- Pt–Ru@PVP nanoparticles can be easily prepared from the co-reduction of corresponding platinum and ruthenium salts by an alcohol reduction method.
- Pt–Ru@PVP nanoparticles are highly efficient catalyst for hydrogen generation from the hydrolysis of AB.
- They provide a record numbers of average TOF value ($308\ mol\ H_2\ mol_{cat}^{-1}\ min^{-1}$) and maximum hydrogen generation rate ($9884\ L\ H_2\ min^{-1}\ (mol_{cat})^{-1}$) for the hydrolysis of AB.
- Activation energy for the catalytic hydrolysis of AB in the presence of Pt–Ru@PVP nanoparticles was calculated as $56.3 \pm 2\ kJ\ mol^{-1}$.
- Pt–Ru@PVP nanoparticles can be regarded as promising catalysts having high activity for practical applications to supply hydrogen from the hydrolysis of AB for proton exchange membrane fuel cells.

Acknowledgment

TEM–EDX and XPS analyses were conducted at the Central Laboratory of Middle East Technical University.

References

[1] D.A.J. Rand, R.M. Dell, J. Power Sources 144 (2005) 568–578.
[2] J. Zhang, T.S. Fisher, J.P. Gore, D. Hazra, P.V. Ramachandran, Int. J. Hydrogen Energy 31 (2006) 2292–2298.
[3] U.S. Department of Energy, Basic research needs for the hydrogen economy, in: Report of the Basic Energy Sciences Workshop on Hydrogen Production, Storage and Use, Office of Science, U.S. Department of Energy, 2003 May 13–15 www.sc.doe.gov/bes/hydrogen.pdf
[4] Energy Information Administration, Annual Energy Outlook 2005 With Projections To 2025, Energy Information Administration, 2005 February www.eia.doe.gov/oiaf/aeo/pdf/0383(2005).pdf
[5] J. Turner, G. Sverdrup, K. Mann, P.G. Maness, B. Kroposki, M. Ghirardi, R.J. Evans, D. Blake, Int. J. Energy Res. 32 (2008) 379–407.
[6] C.H. Liu, B.H. Chen, C.L. Hsueh, J.R. Ku, M.S. Jeng, F. Tsau, Int. J. Hydrogen Energy 34 (2009) 2153–2163.
[7] Q. Zhang, G.M. Smith, Y. Wu, Int. J. Hydrogen Energy 32 (2007) 4731–4735.
[8] Z.H. Lu, Q. Xu, Funct. Mater. Lett. 5 (2012) 1230001.
[9] F.H. Stephens, V. Pons, R.T. Baker, Dalton Trans. 25 (2007) 2613–2626.
[10] M. Yadav, Q. Xu, Energy Environ. Sci. 5 (2012) 9698–9725.
[11] M. Chandra, Q. Xu, J. Power Sources 156 (2006) 190–194.
[12] F. Cheng, H. Ma, Y. Li, J. Chen, Inorg. Chem. 46 (2007) 788–794.
[13] S.B. Kalidindi, U. Sanyal, B.R. Jagirdar, Phys. Chem. Chem. Phys. 10 (2008) 5870–5874.
[14] T. Umegaki, J.M. Yan, X.B. Zhang, H. Shioyama, N. Kuriyama, Q. Xu, J. Power Sources 191 (2009) 209–216.
[15] J.M. Yan, X.B. Zhang, S. Han, H. Shioyama, Q. Xu, Angew. Chem. Int. Ed. 47 (2008) 2287–2289.
[16] T. Umegaki, J.M. Yan, X.B. Zhang, H. Shioyama, N. Kuriyama, Q. Xu, Int. J. Hydrogen Energy 34 (2009) 3816–3822.
[17] Ö. Metin, S. Özkar, Energy Fuels 23 (2009) 3517–3526.
[18] Ö. Metin, Ş. Şahin, S. Özkar, Int. J. Hydrogen Energy 34 (2009) 6304–6313.
[19] J.M. Yan, X.B. Zhang, S. Han, H. Shioyama, Q. Xu, J. Power Sources 194 (2009) 478–481.
[20] J.M. Yan, X.B. Zhang, H. Shioyama, Q. Xu, J. Power Sources 195 (2010) 1091–1094.
[21] J.M. Yan, X.B. Zhang, S. Han, H. Shioyama, Q. Xu, Inorg. Chem. 48 (2009) 7389–7393.
[22] H.B. Dai, L.L. Gao, Y. Liang, X.D. Kang, P. Wang, J. Power Sources 195 (2010) 307–312.
[23] D.G. Tong, X.L. Zeng, W. Chu, D. Wang, P. Wu, J. Mater. Sci. 45 (2010) 2862–2867.
[24] N. Patel, R. Fernandes, G. Guella, A. Miotello, Appl. Catal., B: Environ. 95 (2010) 137–143.
[25] H.L. Jiang, T. Umegaki, T. Akita, X.B. Zhang, M. Haruta, Q. Xu, Chem. Eur. J. 16 (2010) 3132–3137.
[26] Y. Yamada, K. Yano, Q. Xu, S. Fukuzumi, J. Phys. Chem. C 114 (2010) 16456–16462.
[27] M. Rakap, E.E. Kalu, S. Özkar, Int. J. Hydrogen Energy 36 (2011) 254–261.
[28] M. Rakap, E.E. Kalu, S. Özkar, Int. J. Hydrogen Energy 36 (2011) 1448–1455.
[29] Ö. Metin, S. Özkar, S. Sun, Nano Res. 3 (2010) 767–784.
[30] T. Umegaki, J.M. Yan, X.B. Zhang, H. Shioyama, N. Kuriyama, Q. Xu, J. Power Sources 195 (2010) 8209–8214.
[31] B. Kiliç, S. Şencanli, Ö. Metin, J. Mol. Catal. A: Chem. 361–362 (2012) 104–110.
[32] H. Can, Ö. Metin, Appl. Catal., B: Environ. 125 (2012) 304–310.
[33] H.L. Jiang, Q. Xu, J. Mater. Chem. 21 (2011) 13705–13725.
[34] A.K. Singh, Q. Xu, ChemCatChem 5 (2013) 652–676.
[35] N. Toshima, K. Hirakawa, Appl. Surf. Sci. 121-122 (1997) 534–537.
[36] K.S. Eom, K.W. Cho, H.S. Kwon, Int. J. Hydrogen Energy 35 (2010) 181–186.
[37] Z.Q. Tian, S.P. Jiang, Y.M. Liang, P.K. Shen, J. Phys. Chem. B 110 (2006) 5343–5350.
[38] C.D. Wagner, W.M. Riggs, L.E. Davis, J.F. Moulder, B.E. Muilenberg (Eds.), Handbook of X-ray Photoelectron Spectroscopy, Perkin–Elmer Physical Electronics Division, Eden Prairie, 1979, p. 106.
[39] P.V. Ramachandran, P.D. Gagare, Inorg. Chem. 46 (2007) 7810–7817.
[40] S.B. Kalidindi, M. Indirani, B.R. Jagirdar, Inorg. Chem. 47 (2008) 7424–7429.
[41] M. Rakap, S. Özkar, Int. J. Hydrogen Energy 35 (2010) 1305–1312.
[42] C.F. Yao, L. Zhuang, Y.L. Cao, X.P. Hi, H.X. Yang, Int. J. Hydrogen Energy 33 (2008) 2462–2467.
[43] X. Yang, F. Cheng, J. Liang, Z. Tao, J. Chen, Int. J. Hydrogen Energy 34 (2009) 8785–8791.
[44] Ö. Metin, S. Özkar, Int. J. Hydrogen Energy 36 (2011) 1424–1432.
[45] T.J. Clark, G.R. Whittell, I. Manners, Inorg. Chem. 46 (2007) 7522–7527.
[46] F. Durap, M. Zahmakıran, S. Özkar, Appl. Catal., A: Gen. 369 (2009) 53–59.
[47] M. Zahmakıran, S. Özkar, Appl. Catal., B: Environ. 89 (2009) 104–110.
[48] F. Durap, M. Zahmakıran, S. Özkar, Int. J. Hydrogen Energy 34 (2009) 7223–7230.
[49] Q. Xu, M. Chandra, J. Alloys Compd. 446–447 (2007) 729–732.
[50] D. Sun, V. Mazumder, Ö. Metin, S. Sun, ACS Nano 5 (2011) 6458–6464.
[51] Ö. Metin, E. Kayhan, S. Özkar, J.J. Schneider, Int. J. Hydrogen Energy 37 (2012) 8161–8169.
[52] J.M. Yan, X.B. Zhang, T. Akita, M. Haruta, Q. Xu, J. Am. Chem. Soc. 132 (2010) 5326–5327.